Analysis and Design of a Novel 3-DOF Lorentz-Force-Driven DC Planar Motor

Baoquan Kou, He Zhang, and Liyi Li

Department of Electrical Engineering, Harbin Institute of Technology, Harbin 150080, China

In this paper, a novel Lorentz-force-driven DC planar motor with low force ripple is proposed. The magnetic field distribution is calculated analytically by using magnetic surface charge model and image method. The expressions of force and torque are derived based on the Lorentz force law. A method for electromagnetic design of the motor is also discussed. The static force characteristic is measured experimentally. The experiment results are in good agreement with the results of the analysis and simulation.

Index Terms—**Electromagnetic design, Lorentz force, planar motor, static force characteristic.**

I. Introduction

THE PLANAR motor can achieve planar motion directly by using electromagnetic energy. It has attracted increased interest in recent years due to its simple structure, fast response characteristic, and fewer interference factors. So far, many planar motors based on different principles have been proposed. Most of them can be classified into variable reluctance planar motor [1], [2], induction planar motor [3], [4], synchronous permanent magnet planar motor (SPMPM) [5]–[11], and dc planar motor [12]–[16]. Among them, both the variable reluctance planar motor and the induction planar motor have low efficiency, complicated electromechanical characteristics, and complex control strategy, so it is difficult for them to generate planar motion at high speed and high precision. The SPMPM has the advantages of high power density and low loss. However, the three-phase sinusoidal ac with high quality is hard to obtain because of the switching problem of power devices during inversion. So, the force will be influenced by the higher harmonic current. Moreover, the magnetic field generated by magnet arrays is not always in sinusoidal distribution which will result in a nonsinusoidal back electromotive force (EMF). That will also influence the force and increase the force ripple. The dc planar motor is driven by Lorentz force with the features of low force ripple and high positioning accuracy. The output force is in direct proportion to the input current. So, it has been attracting more and more attention in the high-precision positioning occasions, such as semiconductor lithography process, scanning probe microscope, precision manipulation system and precision measurement system.

At present, the combination of voice coil motors (VCM) is usually applied in micro-motion systems to generate planar motion for precision positioning [17], [18]. However, such a structure has some disadvantages such as complicated construction, not centroidal driven, and owning different force characteristics in two orthogonal directions. In addition, the piezoelectric (PZT) actuators applied in ultra-precision planar motion stages were reported in recent years [19]–[21]. But, PZT actuators are difficult to model analytically due to their strongly nonlinear behavior. Moreover, PZT actuators have poor closed-loop controllability compared to Lorentz motors. In contrast, the dc planar motor has many merits over its counterparts.

In this paper, a novel permanent magnet dc planar motor is proposed. The operating principle of the motor is the same as VCM. The translation stroke is ± 1 mm either in the x direction or in the y direction. A uniform air-gap magnetic field is easy to implement in such a short stroke. Moreover, dc with high quality is easy to obtain compared to the three-phase sinusoidal ac. Therefore, the dc planar motor has lower force ripple than SPMPM in terms of force generation principle. Firstly, the basic structure and the operating principle of the motor are introduced. Secondly, the magnetic field analysis is presented using magnetic surface charge model and image method. Thirdly, the analytical expressions of force, torque, and back-EMF are derived. Besides, the design method of the novel dc planar motor is also proposed.

II. Fundamental Structure

The novel dc planar motor has moving magnets and stationary coils. The double-sided structure is applied in order to increase the air-gap magnetic field and magnetic force. As shown in Fig. 1, the mover consists of 24 pieces of magnets and two back irons. The two back irons are connected by several aluminum plates in order to form the air-gap and make it uniform. The stator consists of four square dc coils and a holding plate, and the four coils are glued to the holding plate on the same level.

A. The Driving Unit

The novel dc planar motor is driven by four Lorentz driving units. Fig. 2 shows the configuration of one driving unit. When the direction of the coil current is clockwise, conductors under the magnets No.1 and No.3 will be driven along the x direction and conductors under the magnets No.2 and No.4 will be driven along the $-y$ direction based on the Lorentz force law. Superposing the two forces and fixing the coil, it can be predicted that the mover will move to the top left along the geometrical neutral line of the magnets No.1 and No.2. The direction of force will reverse once the direction of current is reversed.

Manuscript received September 05, 2010; revised October 21, 2010, December 31, 2010, and February 13, 2011; accepted March 12, 2011. Date of publication March 24, 2011; date of current version July 27, 2011. Corresponding author: H. Zhang (e-mail: antonyamanda@163.com).

Color versions of one or more of the figures in this paper are available online at http://ieeexplore.ieee.org.

Digital Object Identifier 10.1109/TMAG.2011.2131671

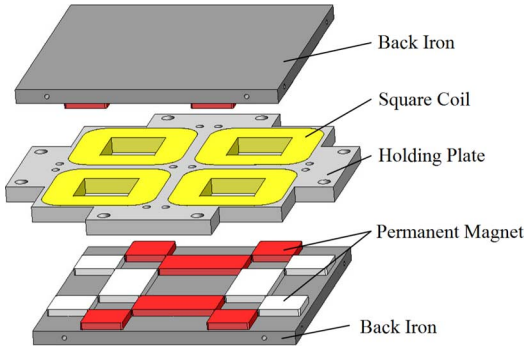

Fig. 1. General 3-D view of the novel dc planar motor.

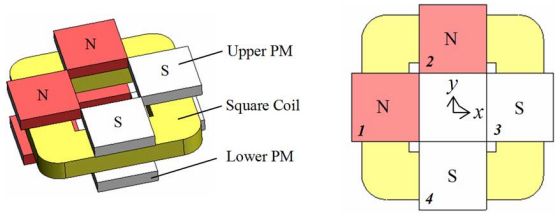

Fig. 2. Lorentz driving unit: (a) 3-D view and (b) top view.

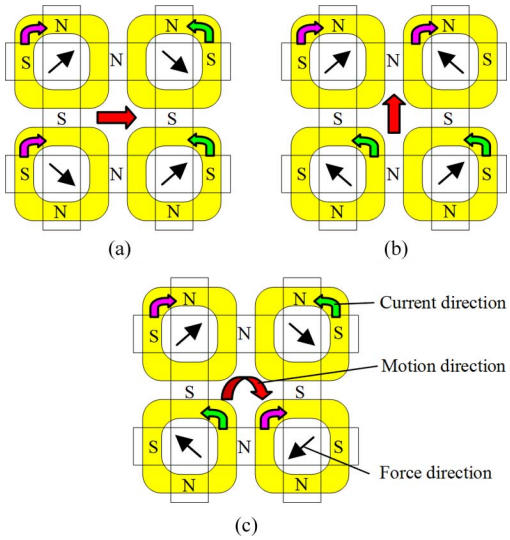

Fig. 3. Analysis of the motor 3-DOF motion: (a) translation in the x direction, (b) translation in the y direction, and (c) rotation about the z axis.

B. Operating Principle of the 3-DOF

The dc planar motor has three degree of freedom (DOF), i.e., translating in the x and y directions and rotating about the z axis. The translation displacement of ± 1 mm in the x and y directions and the rotation degree of $\pm 3°$ about the z axis can be achieved by controlling the four coils currents according to a certain rule. Fig. 3 shows the analysis of the motor 3-DOF motion.

III. Magnetic Field Analysis

A. The Magnetic Field of Permanent Magnets

According to equivalent magnetic charge method [22]–[25], the effect of magnetization for parallel uniform magnetized magnet can be represented by two magnetic charge surfaces on the sides of the permanent magnet, which are perpendicular to the magnetization direction. And the magnetic charge surface density σ_m is equal to the remanent magnetization B_r. Fig. 4 shows the equivalent magnetic charge model of the magnet which is magnetized in the z direction. The length, width, and height of the magnet are $2a$, $2b$, and h_M, respectively, in the x, y, and z direction.

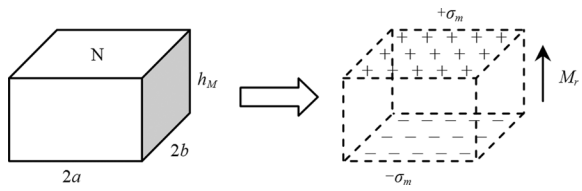

Fig. 4. Equivalent magnetic charge model of PM.

Taking any tiny area ds on the magnetic charge surface, in which the total magnetic charge is

$$dQ_m = \sigma_m ds. \tag{1}$$

Making an analogy with the relationship between electric charge and electric intensity, the magnetic field intensity could be expressed as

$$d\vec{H} = \frac{dQ_m}{4\pi\mu_0 r^2}\vec{a}_r \tag{2}$$

where r is the distance from an arbitrary observation point to the origin. The expression of field strength in z direction generated by the magnetic charge surface is

$$H_z = \int_{-b}^{b}\int_{-a}^{a} \frac{M_r}{4\pi} \times \frac{z}{[(x-x_0)^2+(y-y_0)^2+z^2]^{3/2}} dx_0 \cdot dy_0. \tag{3}$$

Through superposing the equivalent magnetic field of the two magnetic charge surfaces, the analytical expression of the three-dimensional magnetic field generated by a parallel magnetized PM can be obtained as

$$B_z = K \times \begin{bmatrix} \zeta(a-x, b-y, z-h_M)+ \\ \zeta(a-x, b+y, z-h_M)+ \\ \zeta(a+x, b-y, z-h_M)+ \\ \zeta(a+x, b+y, z-h_M)- \\ \zeta(a-x, b-y, z)-\zeta(a-x, b+y, z)- \\ \zeta(a+x, b-y, z)-\zeta(a+x, b+y, z) \end{bmatrix} \tag{4}$$

where

$$K = \frac{\mu_0 M_r}{4\pi} \tag{5}$$

$$\zeta(\zeta_1, \zeta_2, \zeta_3) = \operatorname{arctg}\frac{\zeta_1 \cdot \zeta_2}{\zeta_3 \cdot \sqrt{\zeta_1^2+\zeta_2^2+\zeta_3^2}}. \tag{6}$$

B. The Magnetic Field of Ferromagnetic Boundaries

In the magnetic field generated by PM, ferromagnetic materials will be magnetized and greatly influence the original magnetic field of the PM. So, the final distribution of air-gap field is determined by both PM and ferromagnetic boundaries. Therefore, the image method [26], [27] is adopted to analyze the influence of the ferromagnetic boundaries in order to obtain an accurate air-gap magnetic field. Fig. 5 shows the concept of

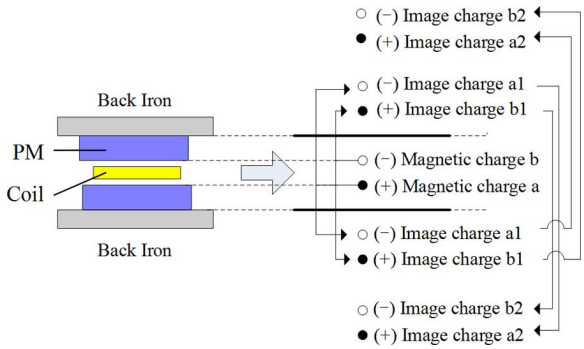

Fig. 5. Concept of image method.

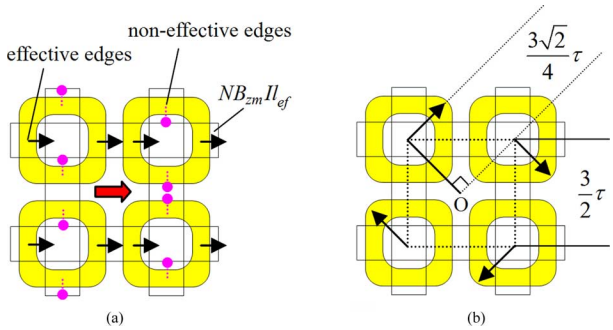

Fig. 6. Force analysis: (a) translation in the x direction and (b) rotation about the z axis.

image method. The distribution rules of image charges can be concluded in the following aspects.

1) For two parallel ferromagnetic boundaries, there are infinite image charge surfaces.
2) Image charge surfaces can be divided into two teams: the positive charge team and the negative charge team.
3) In the same team, the distance between two adjacent charge surfaces is equal to H, and H is the distance between two parallel ferromagnetic boundaries.
4) In the different teams, the distance between a positive charge surface and a negative charge surface is equal to h, and h is the total length of the air-gap.

So, we can transform (4) through the coordinate transformation to gain the image field. The final magnetic field is equal to the sum of the contributions of each image charge and the original charge. The analytical expression of magnetic field generated by a couple of magnets under two parallel ferromagnetic boundaries is derived as

$$B_z = K \times \begin{bmatrix} \zeta(a-x, b-y, z+h/2)+ \\ \zeta(a-x, b+y, z+h/2)+ \\ \zeta(a+x, b-y, z+h/2)+ \\ \zeta(a+x, b+y, z+h/2)- \\ \zeta(a-x, b-y, z-h/2)- \\ \zeta(a-x, b+y, z-h/2)- \\ \zeta(a+x, b-y, z-h/2)- \\ \zeta(a+x, b+y, z-h/2) \end{bmatrix} + K \times \sum_{i=1}^{\infty} \begin{bmatrix} \zeta(a-x, b-y, z+h/2 \pm i \cdot H)+ \\ \zeta(a-x, b+y, z+h/2 \pm i \cdot H)+ \\ \zeta(a+x, b-y, z+h/2 \pm i \cdot H)+ \\ \zeta(a+x, b+y, z+h/2 \pm i \cdot H)- \\ \zeta(a-x, b-y, z-h/2 \pm i \cdot H)- \\ \zeta(a-x, b+y, z-h/2 \pm i \cdot H)- \\ \zeta(a+x, b-y, z-h/2 \pm i \cdot H)- \\ \zeta(a+x, b+y, z-h/2 \pm i \cdot H) \end{bmatrix}. \quad (7)$$

Substituting $x = 0, y = 0, z = 0$ into (7), the magnitude of air-gap magnetic flux density is obtained as

$$B_{zm} = \frac{2\mu_0 M_r}{\pi} \begin{bmatrix} \operatorname{arctg} \frac{l^2}{\frac{h}{2}\sqrt{2l^2+(\frac{h}{2})^2}} \\ +\operatorname{arctg} \frac{l^2}{(\frac{h}{2}\pm H)\sqrt{2l^2+(\frac{h}{2}\pm H)^2}} \\ +\operatorname{arctg} \frac{l^2}{(\frac{h}{2}\pm 2H)\sqrt{2l^2+(\frac{h}{2}\pm 2H)^2}} \end{bmatrix}. \quad (8)$$

C. Analytical Expressions of Force, Torque, and EMF

The proposed dc planar motor is a short-stroke motor. The stroke in x or y direction is ± 1 mm. So, the effective coil edge will be always in the smooth part of magnetic field. When the mover translates in the x (or y) direction, each square coil has two effective edges. The force generated by two effective edges is parallel to x (or y) axis. The force generated by two non-effective edges is perpendicular to x (or y) axis and offset by other coils. As shown in Fig. 6(a), the analytical expression of force (one coil) based on the Lorentz law is

$$F = 2NB_{zm}Il_{\text{ef}} \quad (9)$$

where l_{ef} is the length of effective coil edge.

The analytical expression of back-EMF (one coil) is

$$E = 2NB_{zm}l_{\text{ef}}v \quad (10)$$

where v is the velocity of the mover.

Taking four coils into account, we can obtain the analytical expression of total force:

$$F = 8NB_{zm}Il_{\text{ef}}. \quad (11)$$

As shown in Fig. 6(b), when the mover rotates about the z axis, each square coil has four effective edges. The superposed force of one coil is $\sqrt{2}F$, and the arm of force is $3\sqrt{2} \cdot \tau/4$. So, the expression of torque can be derived as

$$\begin{aligned} T &= 4 \cdot \sqrt{2}F \cdot \frac{3\sqrt{2}}{4}\tau \\ &= 12NB_{zm}Il_{\text{ef}}\tau \end{aligned} \quad (12)$$

where τ is the pole pitch.

IV. Design Method

In the design process of the dc planar motor, we will determine the appropriate dimensions of PM and coil. The main design criterion is to increase the magnetic force.

A. The Main Dimensions' Equation

When the mover is driven, each square coil has four valid edges. Due to the symmetrical structure of the motor, only the cross section of an effective coil edge needs to be analyzed. A

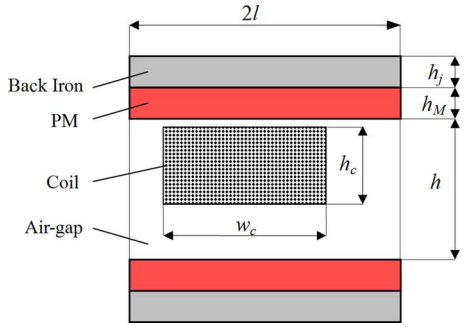

Fig. 7. Side view of analysis model.

2-D modeling approach is utilized in order to simplify design cycle. The longitudinal edge effect is without consideration in this way. It should be noted that the longitudinal edge of planar motor is determined by the direction of conductor.

As shown in Fig. 7, the ampere turns of square coil can be expressed as

$$NI = J_c w_c h_c \tag{13}$$

where J_c is the current density of coil cross section, w_c and h_c denote the width and height of coil cross section, respectively. Compared with the total length of air-gap h, the length of mechanical air-gap is negligible. So, (13) can be approximated as

$$NI = J_c w_c h. \tag{14}$$

For decreasing the force ripple, the coil should be set in the middle of the magnetic field. Then, the width of coil cross section is

$$w_c = C_{fw}\tau \tag{15}$$

where C_{fw} is the flat top width coefficient which is defined as

$$C_{fw} = \frac{W}{\tau} \tag{16}$$

where W is the width range in which the air-gap flux density $B_\delta > kB_{\max}$ as shown in Fig. 9. The coefficient $k = 0.9$ is an appropriate value by taking force and force ripple into consideration.

In addition, the effective edge of coil should be placed under the position where air-gap magnetic field is strong in order to increase the force. Here, we suppose the average length of the conductors is approximately equal to the pole pitch,

$$l_{\text{av}} = \tau. \tag{17}$$

The length of the effective coil edge is

$$l_{\text{ef}} = \alpha_i l_{\text{av}} \tag{18}$$

where α_i is the pole-arc coefficient, defined as the ratio of B_{av} to $B_{\max}$. B_{av} is the average value of air-gap flux density.

By substituting (14), (15), (17), and (18) into (11), the main dimensions' equation can be derived as

$$\frac{\tau^2 h}{F_{em}} = \frac{0.125}{C_{fw}\alpha_i J_c B_\delta}. \tag{19}$$

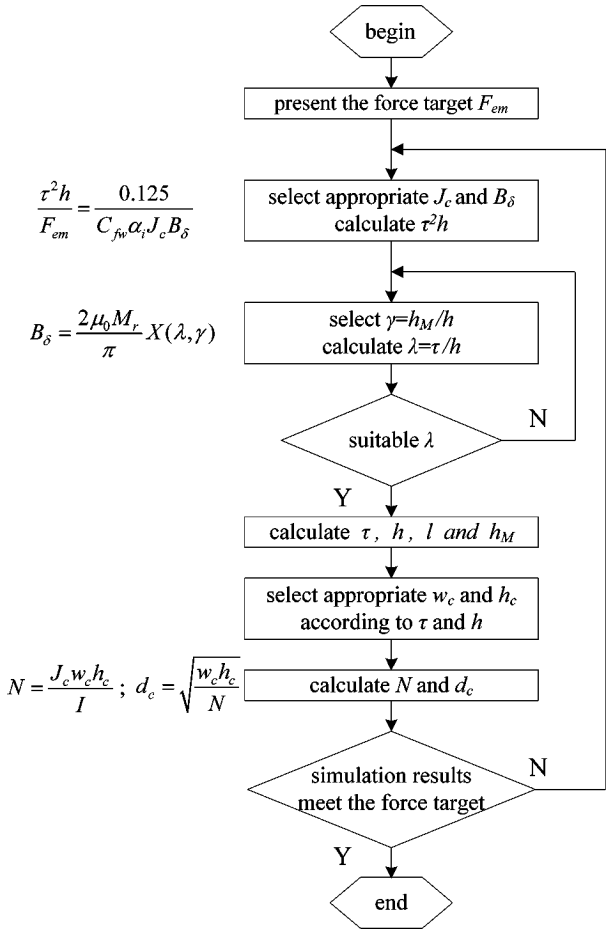

Fig. 8. The design flow chart.

In (19), $\tau^2 h$ is directly proportional to the volume of stator, and it is also related to the volume of the mover. Now, we can estimate the electromagnetic force just by selecting an appropriate electromagnetic load. In other words, when the force target is given, we can estimate the volume of motor just by selecting an appropriate electromagnetic load. So, it can be seen that the pole pitch and the total length of air-gap are the main dimensions of the dc planar motor. The main dimension ratio is defined as

$$\lambda = \frac{\tau}{h}. \tag{20}$$

The design flow chart is given in Fig. 8.

B. The Dimensions of Permanent Magnet

The magnitude of air-gap magnetic flux has been derived in part III, and the expression is

$$B_\delta = \frac{2\mu_0 M_r}{\pi} X(l, h_M, h) \tag{21}$$

where

$$X(l,h_M,h) = \text{arctg}\frac{l^2}{\frac{h}{2}\sqrt{2l^2+\left(\frac{h}{2}\right)^2}} + \text{arctg}\frac{l^2}{\left[\frac{h}{2}\pm(h+2h_M)\right]\sqrt{2l^2+\left[\frac{h}{2}\pm(h+2h_M)\right]^2}}$$

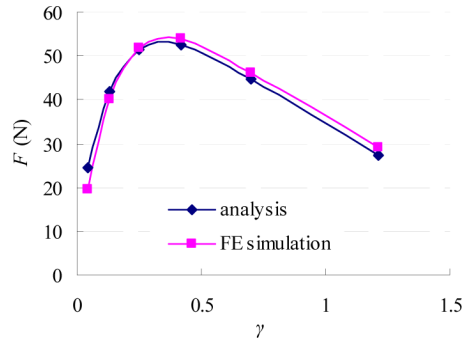

Fig. 9. Variations of force versus γ. ($\tau = 54$ mm, $H = 24$ mm, $J_c = 2.9$ A/mm^2, $\delta = 1.5$ mm).

$$+\operatorname{arctg}\frac{l^2}{\left[\frac{h}{2}\pm 2(h+2h_M)\right]\sqrt{2l^2+\left[\frac{h}{2}\pm 2(h+2h_M)\right]^2}}$$
$$=\operatorname{arctg}\frac{\lambda^2}{4\sqrt{\frac{1}{2}\lambda^2+1}}$$
$$+\operatorname{arctg}\frac{\lambda^2}{4[1\pm 2(1+2\gamma)]\sqrt{\frac{1}{2}\lambda^2+[1\pm 2(1+2\gamma)]^2}}$$
$$+\operatorname{arctg}\frac{\lambda^2}{4[1\pm 4(1+2\gamma)]\sqrt{\frac{1}{2}\lambda^2+[1\pm 4(1+2\gamma)]^2}}$$
$$=X(\lambda,\gamma) \tag{22}$$

where γ is the ratio between the thickness of permanent magnet and the total length of air gap, i.e.,

$$\gamma=\frac{h_M}{h}. \tag{23}$$

Equation (22) shows that the magnitude of air-gap magnetic flux is only determined by λ and γ. Firstly, after selecting the suitable J_c and B_δ, we can calculate $\tau^2 h$ according to (19). Secondly, we should select suitable γ, and λ can be calculated according to (22). The thickness of permanent magnet, the pole pitch, and the total length of air gap will be calculated once $\tau^2 h$, λ and γ are obtained. In order to maximize the force, we need to find the optimal γ. Fig. 9 shows the variation of the force versus γ when $\tau = 54$ mm, $H = 24$ mm, $J_c = 2.9$ A/mm^2, and $\delta = 1.5$ mm. The optimization can be obtained by the following equation:

$$\frac{\partial F}{\partial \gamma}=0. \tag{24}$$

Permanent magnets in the novel dc planar motor are all square. So, the relationship between edge length of magnet and pole pitch is

$$2l=\frac{\tau}{2}. \tag{25}$$

C. The Dimensions of Coil

To determine appropriate coil dimensions, the distribution of air-gap magnetic field needs to be analyzed. As the double-sided

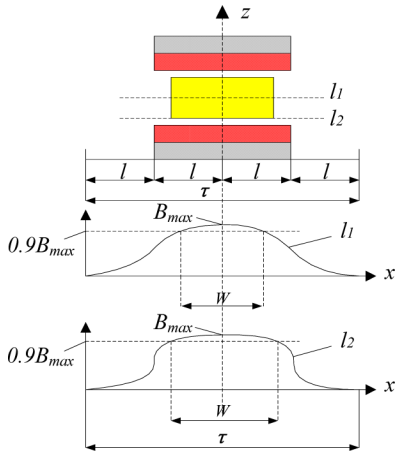

Fig. 10. Magnetic field distribution in the middle of air-gap and on the surface of magnet.

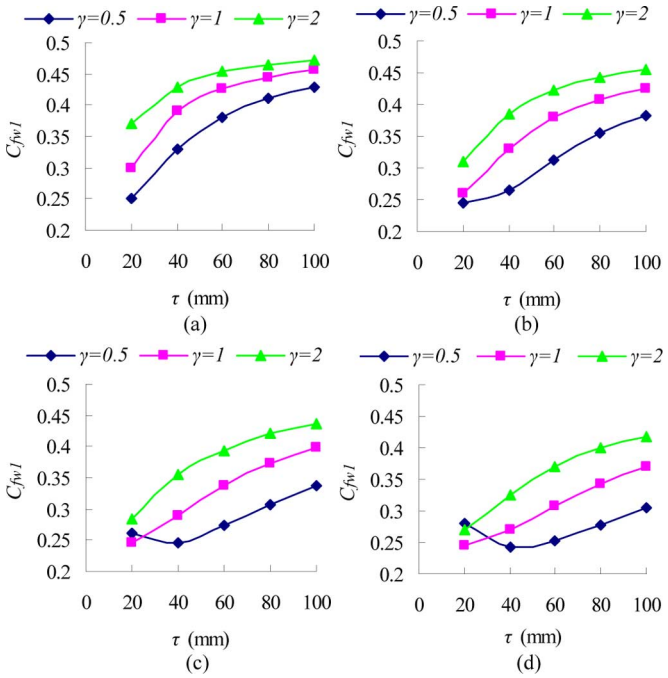

Fig. 11. Flat top width coefficient C_{fw1}: (a) $h_M = 3$ mm, (b) $h_M = 5$ mm, (c) $h_M = 7$ mm, and (d) $h_M = 9$ mm.

structure is applied, the total length of air-gap is relatively large. So, the magnetic field distribution in the middle of air-gap is different from the magnetic field distribution on the surface of magnet. As shown in Fig. 10, the descent speed of flux density in the middle of air-gap is fast, but flux density on the surface of magnet starts to decrease until getting close to the fringe of magnet. Therefore, the variation of magnetic field along the z axis should be taken into consideration when calculating the width of coil.

In this paper, the flat top width coefficient is used to indicate the smoothness of magnetic field distribution. The flat top width coefficient in the middle of air-gap is C_{fw1}, and the flat top width coefficient on the surface of magnet is C_{fw2}. According to (7), the coefficient with different dimensions of magnet can be calculated, as shown in Figs. 11 and 12.

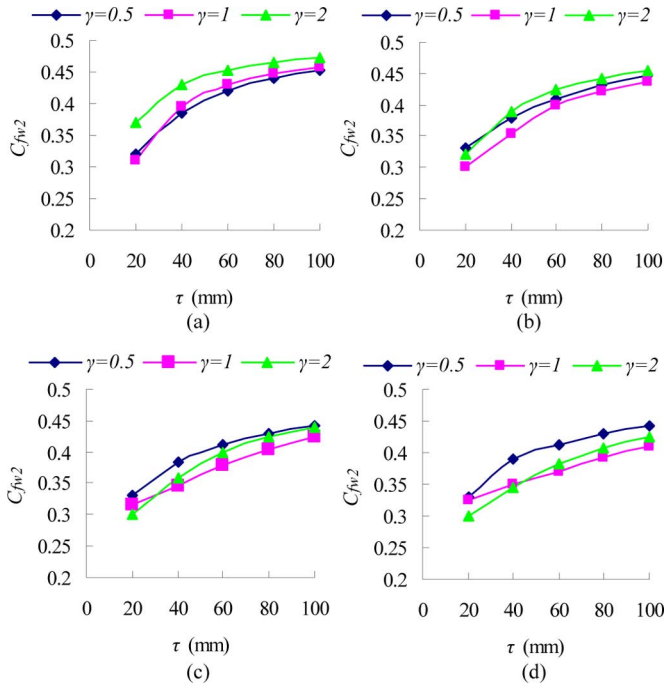

Fig. 12. Flat top width coefficient C_{fw2}: (a) $h_M = 3$ mm, (b) $h_M = 5$ mm, (c) $h_M = 7$ mm, and (d) $h_M = 9$ mm.

It can be found that both C_{fw1} and C_{fw2} will increase with the increment of pole pitch. However, the difference is that C_{fw1} is greatly influenced by the ratio of γ, and C_{fw2} is not obviously affected by the ratio of γ.

The coil width can be expressed as

$$w_c = \frac{C_{fw1} + C_{fw2}}{2}\tau. \tag{26}$$

The length of mechanical air-gap can be selected within 1–2 mm, and the height of coil is

$$h_c = h - 2\delta. \tag{27}$$

When the dimensions of coil cross section have been determined, the turns per coil can be calculated by

$$N = \frac{J_c w_c h_c}{I}. \tag{28}$$

It is assumed that all the conductors of coil form a regular square arrangement; in other words, the centers of conductors in each column are in a straight line. So, the diameter of enamel insulated wire is

$$d_c = \sqrt{\frac{w_c h_c}{N}}. \tag{29}$$

V. Simulation and Experiment

A prototype of the dc planar motor is shown in Fig. 13. The parameters of the prototype motor are shown in Table I.

The armature reaction can be neglected due to ironless structure and long air-gap. Fig. 14 shows the magnetic field simulation result in no-load condition. Fig. 14(b) indicates that the analytical values of air-gap flux density are in good agreement with those of the simulation.

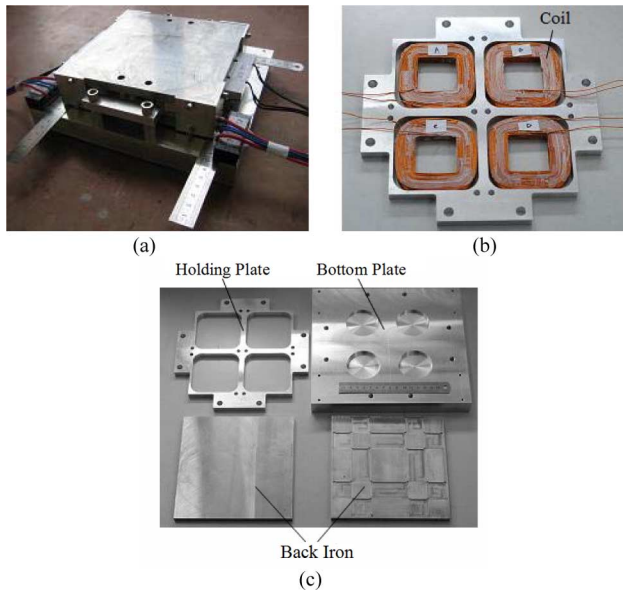

Fig. 13. Prototype of dc planar motor: (a) general view, (b) coils and holding plate, and (c) main parts.

TABLE I
Dimensions of Prototype

Item		Symbol	Value	Unit
Magnet	type	N38		
	remanent magnetization	B_r	1.254	T
	edge length	$2l$	27	mm
	thickness	h_M	5.5	mm
Coil	number of turns	N	276	turns
	width of cross section	w_c	17.8	mm
	height of cross section	h_c	9.6	mm
	diameter	d_c	0.76	mm
	resistance	R	2.35	Ω
	inductance	L	4.59	mH
Pole pitch		τ	54	mm
Pole-arc coefficient		α_i	0.515	--
Length of mechanical air-gap		δ	1.5	mm
Total length of air-gap		h	13	mm
Dimensions of back iron			168×168×9	mm
Dimensions of bottom plate			220×240×35	mm

Fig. 15 shows the static force measurement devices of dc planar motor. Four groups of stainless steel balls between the mover and the bottom plate are used to support the mover to achieve planar motion. The static force is measured using pressure sensor (T90194) and P-V converter (DKMO2A). Fig. 16 shows the force-current relation. The static force characteristics in the x and y directions both increase linearly with the increment of current. In this paper, the analysis force is calculated by (11). And, the simulation force is obtained by the FEM software Ansoft3D.

Fig. 17 shows the relation between the force and displacement. The analysis force is a constant during the whole travel range because it's assumed that B is equal to B_{zm}. But, fringing effect will be considered in 3-D FEM simulation. So, both simulation and experiment forces show a trend of slightly decrease once the mover travels beyond the stroke of ±1 mm. When the

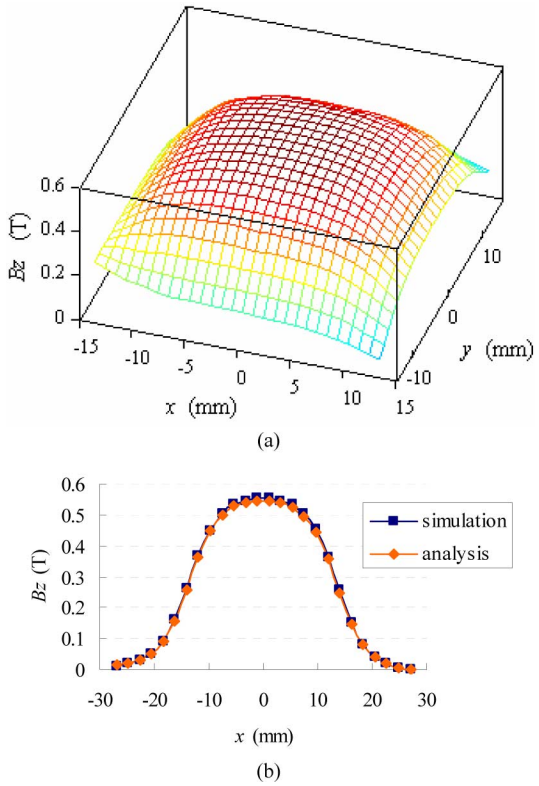

Fig. 14. Simulation result of no-load air gap magnetic field: (a) 3-D view and (b) correlation curve.

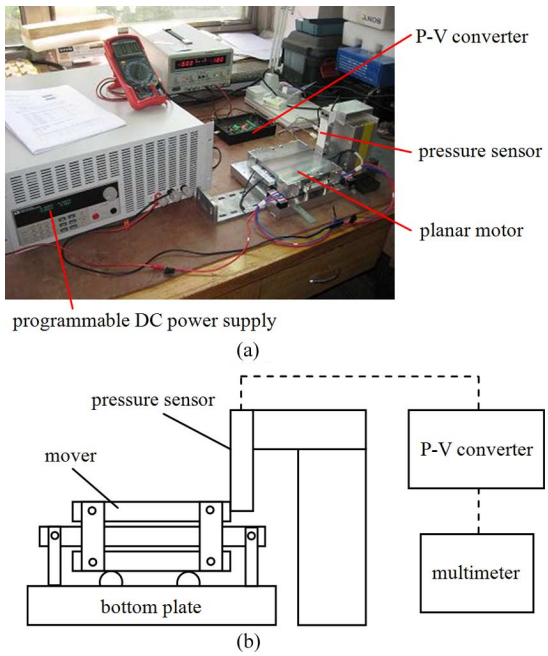

Fig. 15. The static force measurement devices: (a) experimental platform and (b) schematic diagram.

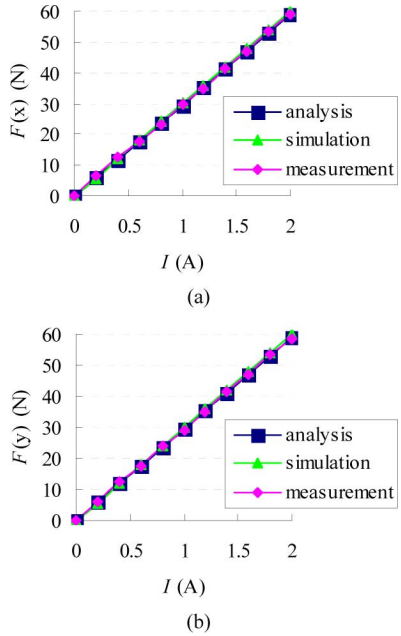

Fig. 16. The force versus current: (a) in the x direction and (b) in the y direction.

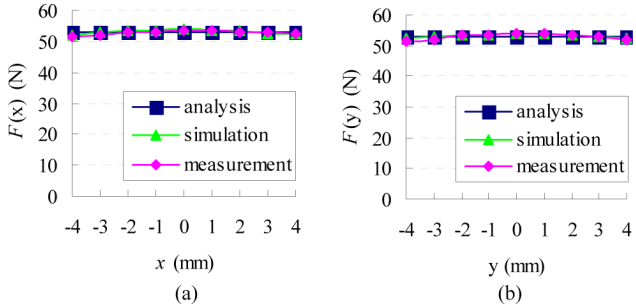

Fig. 17. The force versus displacement: (a) in the x direction and (b) in the y direction.

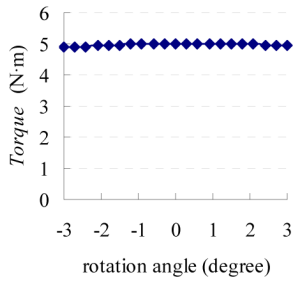

Fig. 18. The torque versus rotation angle.

mover travels within the stroke of ± 1 mm, it can be calculated by simulation that the force ripple is 0.59% in the x direction and 0.33% in the y direction. The measured force ripple in Fig. 17 is 0.36% in the x direction and 0.72% in the y direction.

The motor will generate rotation under the effect of torque. The rotation angle is no longer zero and the relative position between the mover and the stator will change. Fig. 18 shows the curve of the torque versus rotation angle obtained from the simulation. The torque has little change when the rotation angle is within the range of $\pm 3°$.

The rotation angle not only affects the torque, but also influences the force. Fig. 19 shows the curve of the force versus rotation angle obtained from the simulation when mover travels in the x direction. The force in the moving direction varies slightly, but the force perpendicular to the moving direction increases

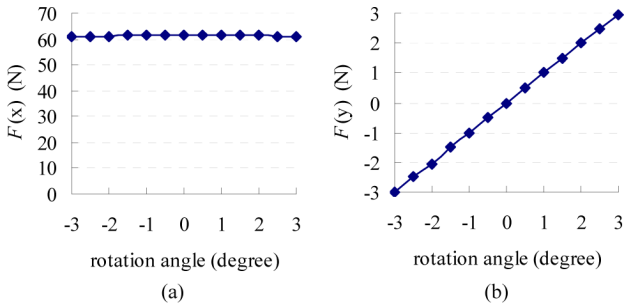

Fig. 19. The force versus rotation angle: (a) in the moving direction and (b) perpendicular to the moving direction.

with the increment of rotation angle. When the angle is $\pm 3°$, F (y) has already reached ± 3 N respectively.

VI. Conclusion

In this paper, a novel dc planar motor was proposed. The motor has low force ripple. The analytical expressions of the air-gap magnetic field and the propulsion force were provided. Also, the design method of the motor was presented. The static force characteristics experiment was performed to validate the analytical and simulation results. The following conclusions can be drawn:

1) The FEM simulation results of magnetic field distribution are in good agreement with the analytical ones. It verifies the validity of analytical model.
2) The dc planar motor proposed in this paper has a good static force characteristic. The output force is in direct proportion to the input current.
3) Force ripples are less than 1% when mover travels within ± 1 mm either in the x direction or in the y direction. It demonstrates that the force nearly maintains constant within the stroke of translation. So, it is easy to control.
4) Propulsion force and torque are not appreciably affected by rotation angles. However, the disturbing force perpendicular to the moving direction is proportional to rotation angles.

This paper focuses mainly on the electromagnetic characteristic of the 3-DOF Lorentz-force-driven motor. However, some relevant issues including the thermal characteristic, the low-friction bearing, and the high precision multidimension measurement also need to be considered for high precision positioning. In future work, we will adopt water cooling to lower the temperature rise of winding. Air bearing or magnetic suspension will be applied to minimize the bearing friction. Furthermore, the precision measurement system composed of laser interferometer and capacitance probe will be used for positioning performance improvement.

Acknowledgment

The work described in this paper was supported by the National S&T Major Project (2009ZX02207-001) and Program for New Century Excellent Talents in University (NCET-08-0158).

References

[1] E. R. Pelta, "Two-axis Sawyer motor for motion systems," *IEEE Contr. Syst. Mag.*, vol. 7, no. 5, pp. 20–24, Oct. 1987.
[2] J. F. Pan, N. C. Cheung, W. C. Gan, and S. W. Zhao, "A novel planar switched reluctance motor for industrial applications," *IEEE Trans. Magn.*, vol. 42, no. 10, pp. 2836–2839, Oct. 2006.
[3] P. Dittrich and D. Radeck, "3-DOF planar induction motor," in *Proc. IEEE Electro/Information Technology Conf.*, May 7–10, 2006, pp. 81–86.
[4] N. Fujii and M. Fujitake, "Two-dimensional drive characteristics by circular-shaped motor," *IEEE Trans. Ind. Appl.*, vol. 35, no. 4, pp. 803–809, Jul./Aug. 1999.
[5] H. S. Cho and H. K. Jung, "Analysis and design of synchronous permanent-magnet planar motors," *IEEE Trans. Energy Convers.*, vol. 17, no. 4, pp. 492–499, Dec. 2002.
[6] J. de Boeij, E. Lomonova, and A. Vandenput, "Modeling ironless permanent-magnet planar actuator structures," *IEEE Trans. Magn.*, vol. 42, no. 8, pp. 2009–2016, Aug. 2006.
[7] W. J. Kim and D. L. Trumper, "High-precision magnetic levitation stage for photolithography," *Precision Eng.*, vol. 22, no. 2, pp. 66–77, Apr. 1998.
[8] J. Y. Cao, Y. Zhu, W. C. Gan, J. S. Wang, W. S. Yin, and G. H. Duan, "A novel synchronous permanent magnet planar motor and its model for control applications," *IEEE Trans. Magn.*, vol. 41, no. 6, pp. 2156–2163, Jun. 2005.
[9] Y. Ueda and H. Ohsaki, "A planar actuator with a small mover traveling over large yaw and translational displacements," *IEEE Trans. Magn.*, vol. 44, no. 5, pp. 609–616, May 2008.
[10] J. W. Jansen, C. M. M. van Lierop, E. A. Lomonova, and A. J. A. Vandenput, "Modeling of magnetically levitated planar actuators with moving magnets," *IEEE Trans. Magn.*, vol. 43, no. 1, pp. 15–25, Jan. 2007.
[11] J. C. Comper, "Electro-dynamic planar motor," *Precision Eng.*, vol. 28, no. 2, pp. 171–180, Apr. 2004.
[12] W. Gao, S. Dejima, H. Yanai, K. Katakura, S. Kiyono, and Y. Tomita, "A surface motor-driven planar motion stage integrated with an $XY\theta_Z$ surface encoder for precision positioning," *Precision Eng.*, vol. 28, no. 3, pp. 329–337, Jul. 2004.
[13] W. J. Kim, S. Verma, and H. Shakir, "Design and precision construction of novel magnetic-levitation-based multi-axis nanoscale positioning systems," *Precision Eng.*, vol. 31, no. 4, pp. 337–350, Oct. 2007.
[14] A. Molenaar, E. H. Zaaijer, and H. F. van Beek, "A novel low dissipation long stroke planar magnetic suspension and propulsion stage," in *Proc. 6th Int. Symp. on Magnetic Bearings*, Cambridge, MA, 1998, pp. 650–659, MIT.
[15] Z. P. Zhang and C. H. Menq, "Six-axis magnetic levitation and motion control," *IEEE Trans. Robot.*, vol. 23, no. 2, pp. 15–25, Apr. 2007.
[16] K. S. Jung and Y. S. Baek, "Study on a novel contact-free planar system using direct drive DC coils and permanent magnets," *IEEE/ASME Trans. Mechatronics.*, vol. 7, no. 2, pp. 35–43, Mar. 2002.
[17] M. Y. Chen, M. J. Wang, and L. C. Fu, "A novel dual-axis repulsive Maglev guiding system with permanent magnet: Modeling and controller design," *IEEE/ASME Trans. Mechatronics.*, vol. 8, no. 1, pp. 77–86, Mar. 2003.
[18] J. Lei, X. Luo, X. D. Chen, and T. H. Yan, "Modeling and analysis of a 3-DOF Lorentz-force-driven planar motion stage for nanopositioning," *Mechatronics.*, vol. 20, no. 5, pp. 553–565, May 2010.
[19] Y. F. Wu and Z. Y. Zhou, "An $XY\theta$ mechanism actuated by one actuator," *Mech. Mach. Theory*, vol. 39, no. 10, pp. 1101–1110, Oct. 2004.
[20] W. Y. Jywe, Y. R. Jeng, C. H. Liu, Y. F. Teng, C. H. Wu, H. S. Wang, and Y. J. Chen, "A novel 5DOF thin coplanar nanometer-scale stage," *Precision Eng.*, vol. 32, no. 4, pp. 239–250, Oct. 2008.
[21] H. S. Kim and Y. M. Cho, "Design and modeling of a novel 3-DOF precision micro-stage," *Mechatronics*, vol. 19, no. 5, pp. 598–608, Aug. 2009.
[22] R. Ravaud, G. Lemarquand, V. Lemarquand, and C. Depollier, "Analytical calculation of the magnetic field created by permanent-magnet rings," *IEEE Trans. Magn.*, vol. 44, no. 8, pp. 1982–1989, Aug. 2008.
[23] R. Ravaud, G. Lemarquand, V. Lemarquand, and C. Depollier, "Permanent magnet couplings: Field and torque three-dimensional expressions based on the coulombian model," *IEEE Trans. Magn.*, vol. 45, no. 4, pp. 1950–1958, Apr. 2009.

[24] G. Y. Xiong and S. A. Nasar, "Analysis and field characteristic analysis field and forces in a permanent magnet linear synchronous machine based on the concept of magnetic charge," *IEEE Trans. Magn.*, vol. 25, no. 3, pp. 2713–2719, May 1989.
[25] S. A. Nasar and G. Y. Xiong, "Determination of the field of a permanent-magnet disk machine using the concept of magnetic charge," *IEEE Trans. Magn.*, vol. 24, no. 3, pp. 2038–2044, May 1988.
[26] S. H. Lee, S. B. Park, S. O. Kwon, J. Y. Lee, J. J. Lee, J. P. Hong, and J. Hur, "Characteristic analysis of the slotless axial-flux type brushless dc motors using image method," *IEEE Trans. Magn.*, vol. 42, no. 4, pp. 1327–1330, Apr. 2006.
[27] T. F. Chan and L. L. Lai, "Computation of air-gap field in an axial-flux permanent-magnet machine using the method of images," in *Proc. IEEE Electro Machines and Drive Conf.*, May 3–6, 2009, pp. 1647–1651.

Baoquan Kou (M'09) received the B.E. and D.E. degrees from Harbin Institute of Technology, Harbin, China, in 1992 and 2004, respectively, and the M.E. degree from Chiba Institute of Technology, Chiba, Japan, in 1995.

He worked in the mobile station for the post-doctors of HIT from 2005 to 2007. Since 2007, he has been Professor in the School of Electrical Engineering and Automation, HIT. His research areas are electric drive of electric vehicles, linear motors and linear electromagnetic drives, control of the power quality, and superconducting motors.

He Zhang received the B.E. and M.E. degrees from Harbin Institute of Technology, Harbin, China, in 2008 and 2010, respectively.

Since 2010, he has been with the Institute of Electromagnetic and Electronic Technology, Harbin Institute of Technology, as a doctoral candidate. His research areas are planar motors of high positioning accuracy and high response.

Liyi Li (M'09) received the B.E., M.E., and D.E. degrees from Harbin Institute of Technology, Harbin, China, in 1991, 1995, and 2001, respectively.

From 1991 to 1993, he worked in the Science and Technology Development General Company of HIT. From 2002 to 2004, he worked in the mobile station for the post-doctors of Dalian University of Technology, Dalian, China. Since 2004, he has been Professor in the School of Electrical Engineering and Automation, HIT. His research areas are control and drive of linear electromagnetic systems, linear electromagnetic launch, accumulation of electric energy, and superconducting motors.